

Supporting Information

# Nanotopographical Modulation of Cell Function through Nuclear Deformation

Kai Wang,<sup>†</sup> Allison Bruce,<sup>†</sup> Ryan Mezan,<sup>†</sup> Anand Kadiyala,<sup>‡</sup>

Liyang Wang,<sup>§</sup> Jeremy Dawson,<sup>‡</sup> Yon Rojanasakul,<sup>||</sup> and Yong Yang<sup>\*,†</sup>

<sup>†</sup>Department of Chemical Engineering, West Virginia University, Morgantown, WV 26506,  
United States

<sup>‡</sup>Lane Department of Computer Science and Electrical Engineering, West Virginia University,  
Morgantown, WV 26506, United States

<sup>§</sup>Pathology and Physiology Research Branch, National Institute for Occupational Safety and  
Health, Morgantown, West Virginia 26505, United States

<sup>||</sup>Department of Basic Pharmaceutical Sciences, West Virginia University, Morgantown, WV  
26506, United States

\* Corresponding author

Email address: [yong.yang@mail.wvu.edu](mailto:yong.yang@mail.wvu.edu)

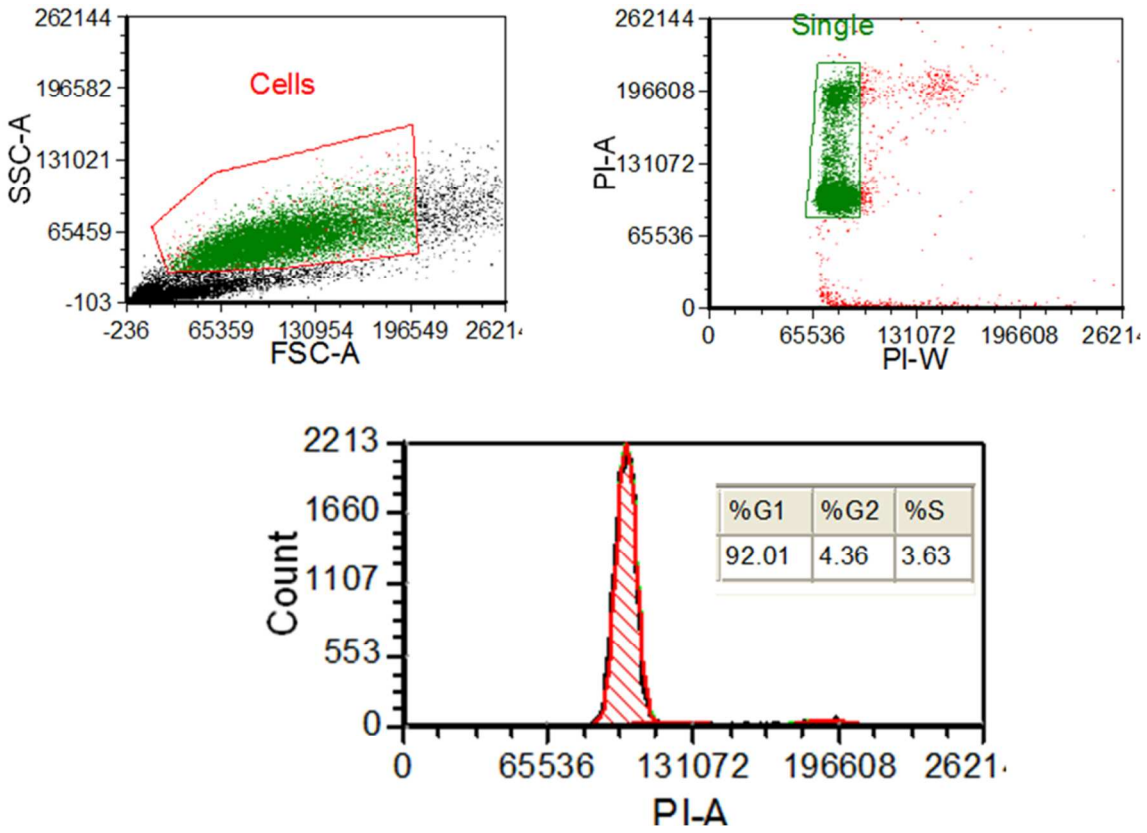


**Figure S1.** Flow cytometry analysis of cell cycle synchronization of the fibroblasts.

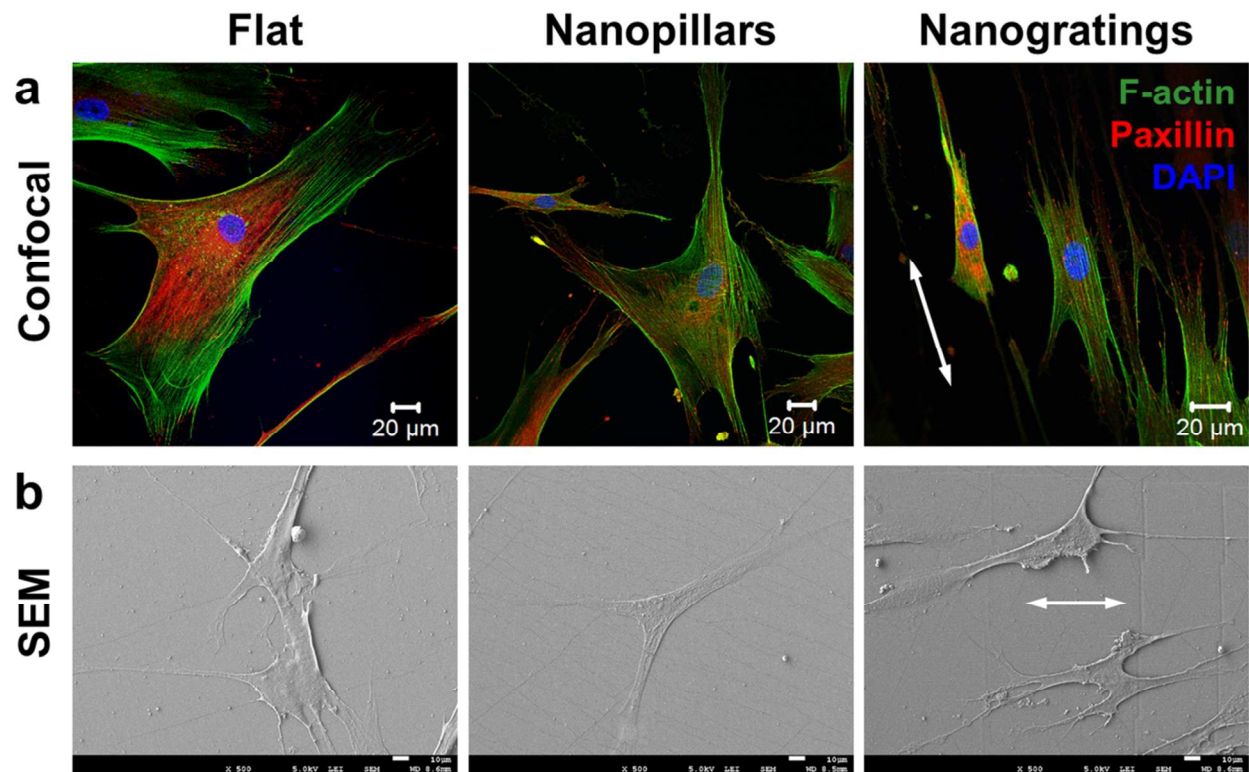


**Figure S2.** Cell spreading on nanotopographies. (a) Immunofluorescence and (b) SEM images of fibroblasts grown on the flat control surface, nanopillars (NP 300-1.9X-150) and nanogratings (NG 500-1X-150). (a) The nuclei were stained with DAPI in blue, the actin filaments were stained with phalloidin in green, and focal adhesions were stained with paxillin in red. (b) The scale bars are 10  $\mu\text{m}$ . The white arrows point to the nanograting orientation.

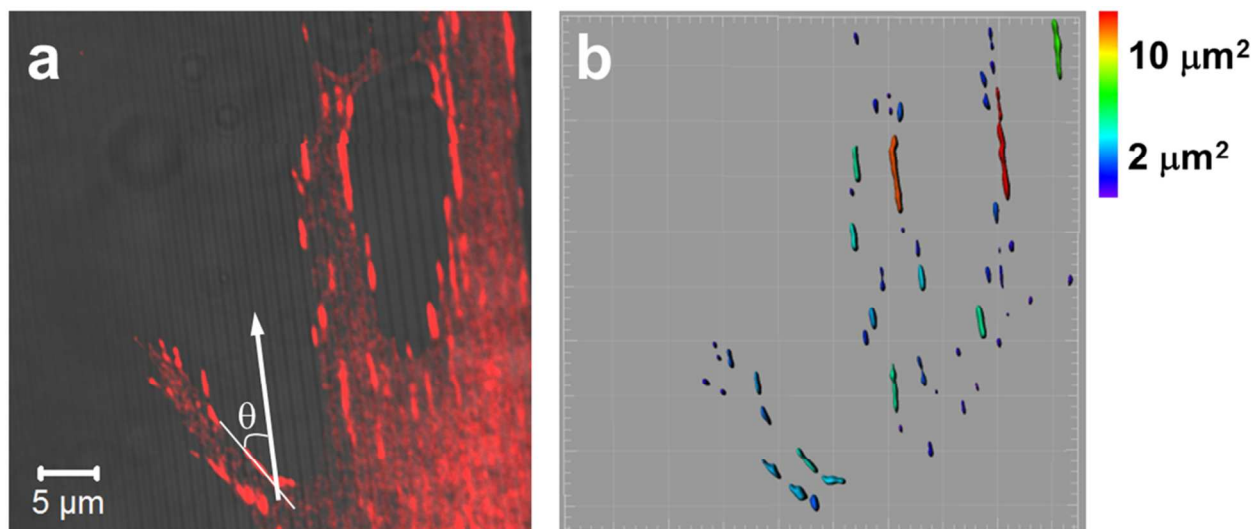


**Figure S3.** Image analysis of focal adhesions. (a) Overlay of confocal and bright-field images of focal adhesion protein paxillin (red). The alignment angle is defined by the angle between the major axis of focal adhesions (thin white line) and the nanograting direction (white arrow). (b) Imaris image of focal adhesions extracted from (a). Focal adhesions of different size are labelled using different colors.

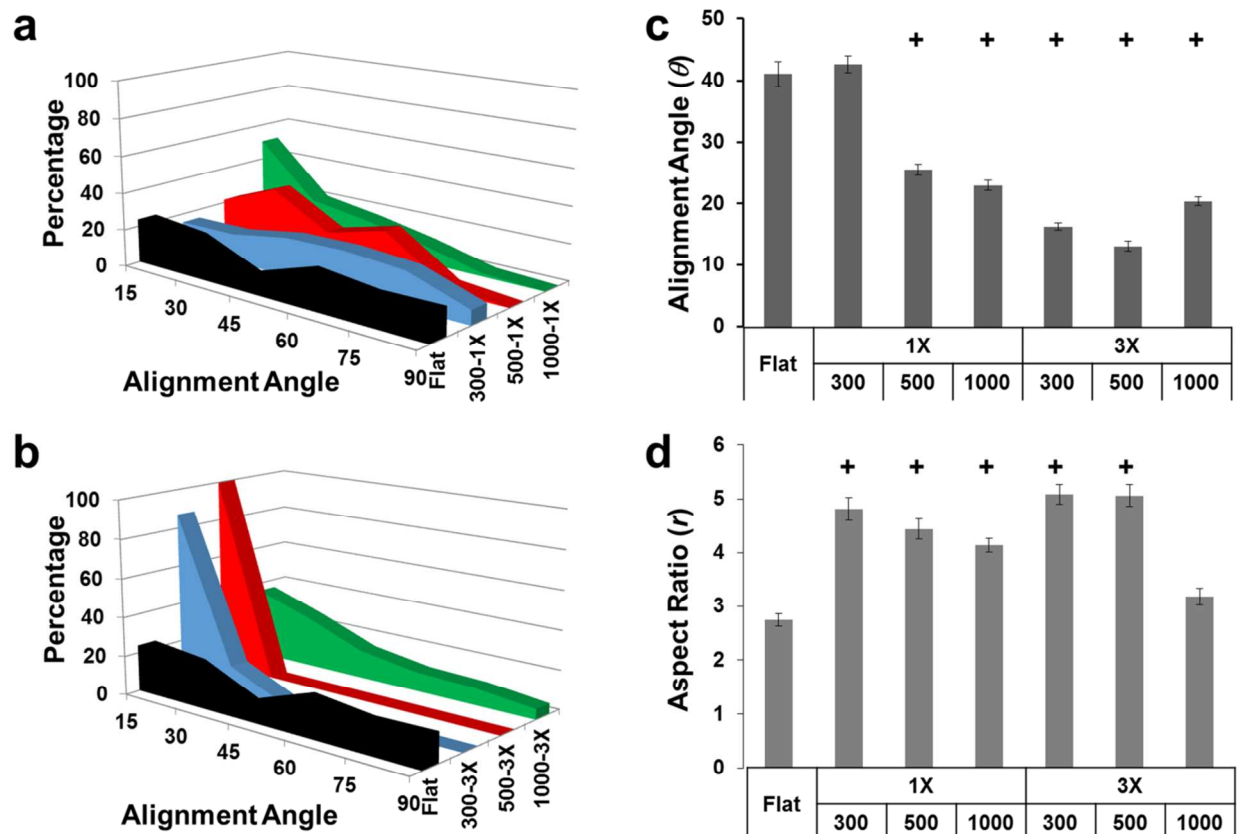


**Figure S4.** Summary of alignment and elongation of focal adhesions on nanogratings of 150 nm in height. (a) Alignment angle distribution of focal adhesions on the nanogratings with a spacing of 1X linewidth. (b) Alignment angle distribution of focal adhesions on the nanogratings with a spacing of 3X linewidth. (c) Effects of nanogratings on the focal adhesions alignment. (d) Effects of nanogratings on the elongation (aspect ratio) of focal adhesions. Significant difference from the flat controls is indicated by + where  $p < 0.001$ .

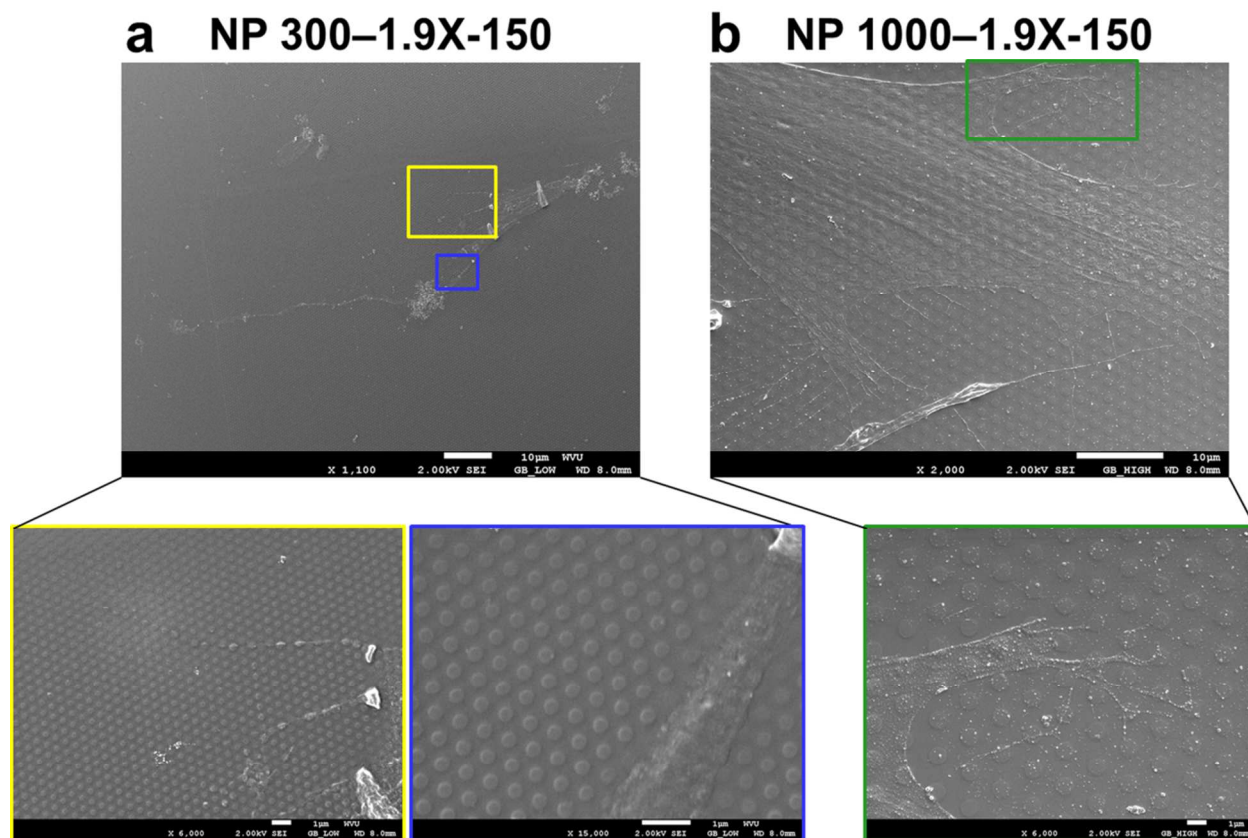


**Figure S5.** SEM images of fibroblasts grown on (a) NP 300-1.9X-150 and (b) NP 1000-1.9X-150. The boxed area was enlarged to detail the cell-nanopillar interactions. The scale bars in the boxed area are 1  $\mu\text{m}$ .

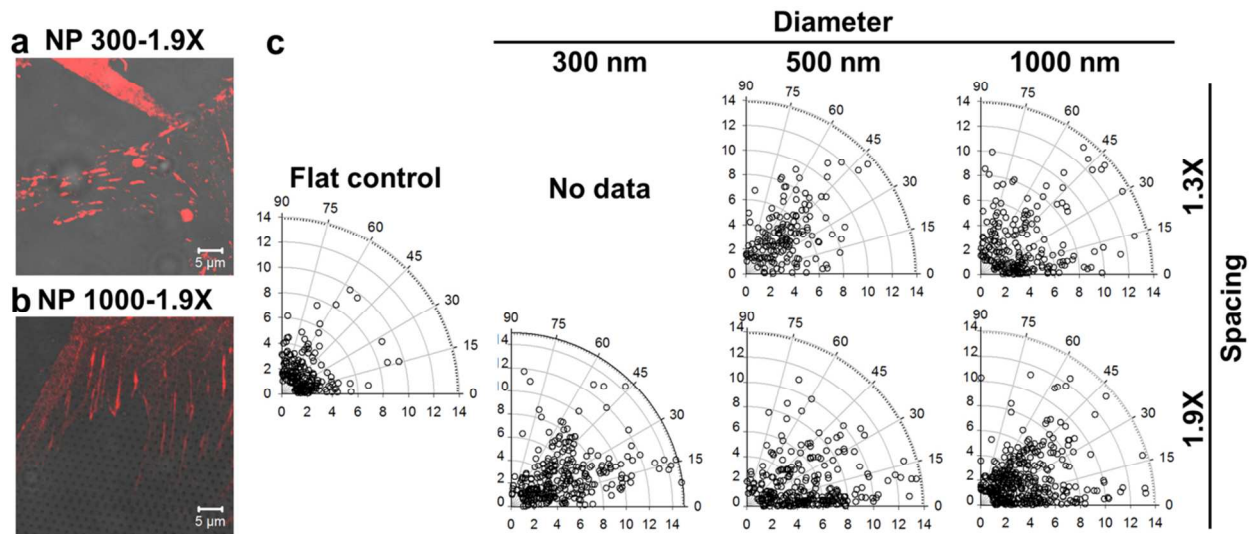


**Figure S6.** Alignment and elongation of focal adhesions on nanopillars of 150 nm in height. (a, b) Overlay of the confocal image of paxillin and the bright field image of nanopillars for the fibroblasts on (a) NG 300-1.9X and (b) NG 1000-1.9X. (c) Polar plots of focal adhesion alignment (angular coordinate) and elongation (radial coordinate) of the fibroblasts on nanogratings as well as the flat control.

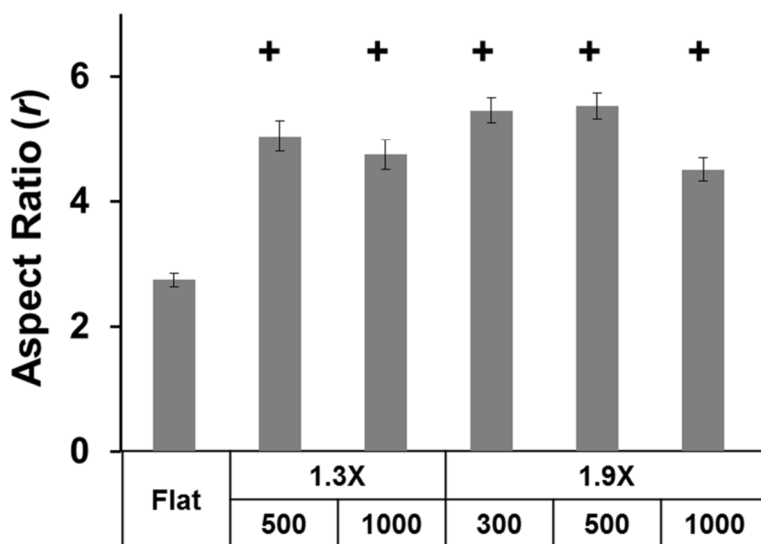


**Figure S7.** Effects of nanopillars on the focal adhesions elongation. Significant difference from the flat controls is indicated by + where  $p < 0.001$ .

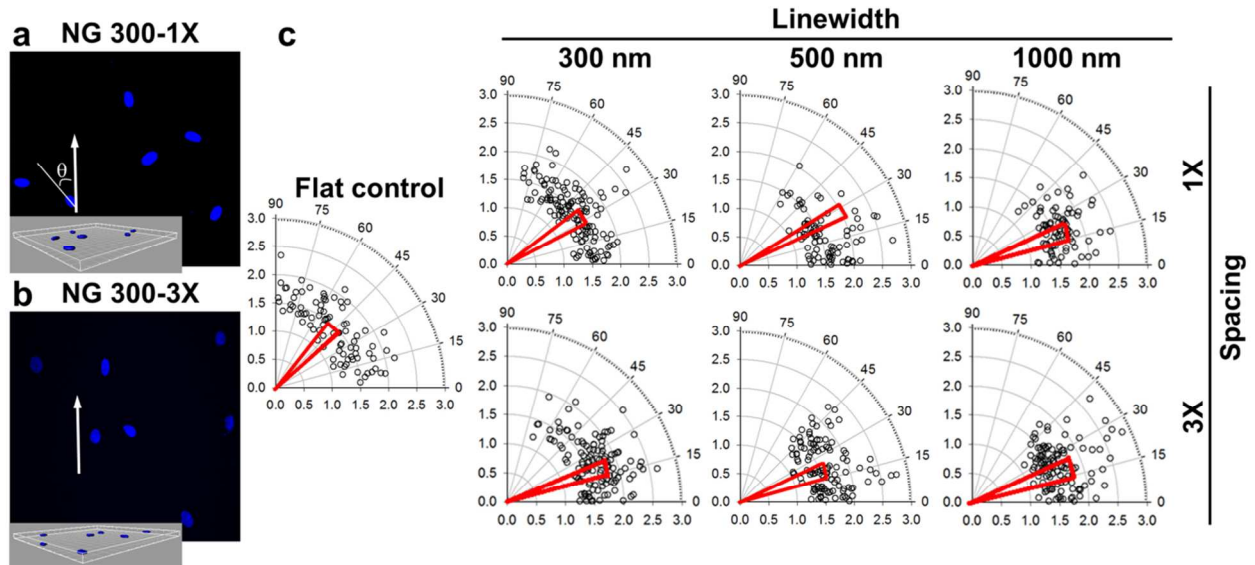


**Figure S8.** Nuclear alignment and elongation on nanogratings of 150 nm in height. (a, b) Confocal images of nuclei on (a) NG 300-1X and (b) NG 300-3X. The insets are 3-D reconstruction images. The alignment angle was defined by the angle between the major axis of the nucleus (thin white line) and the nanograting direction (white arrow). (c) Polar plots of nuclear alignment (angular coordinate) and elongation (radial coordinate) of the fibroblasts on nanogratings as well as the flat control.

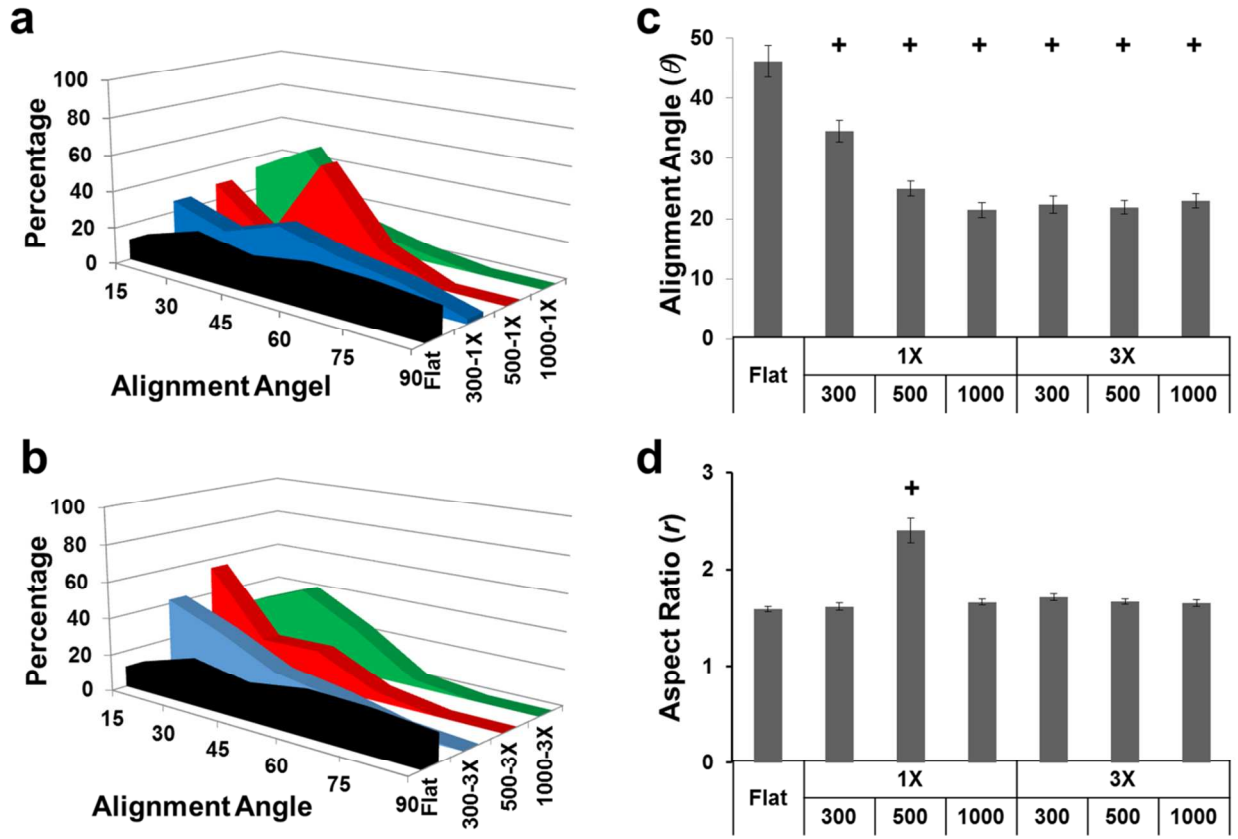


**Figure S9.** Summary of nuclear alignment and elongation of fibroblasts on nanogratings of 150 nm in height. (a) Nuclear alignment angle distribution on the nanogratings with a spacing of 1X linewidth. (b) Nuclear alignment angle distribution on the nanogratings with a spacing of 3X linewidth. (c) Effects of nanogratings on the nuclear alignment. (D) Effects of nanogratings on the nuclear elongation (aspect ratio). Significant difference from the flat controls is indicated by + where  $p < 0.001$ .

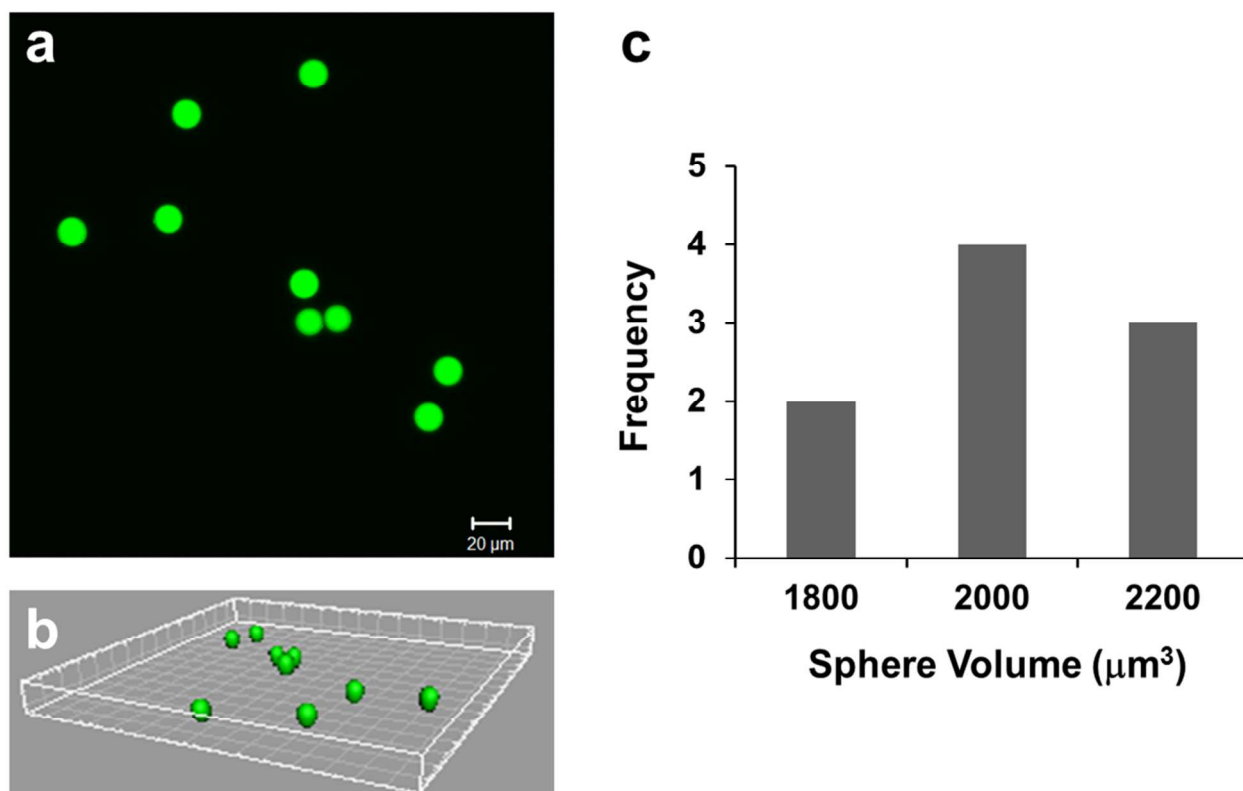


**Figure S10.** Validation of confocal z-stack measurement of nuclear volume. (a) Confocal and (b) Imaris 3-D reconstruction images of FITC-spheres of  $15.4 \pm 0.13 \mu\text{m}$ . (c) Volumetric distribution of FITC-spheres.

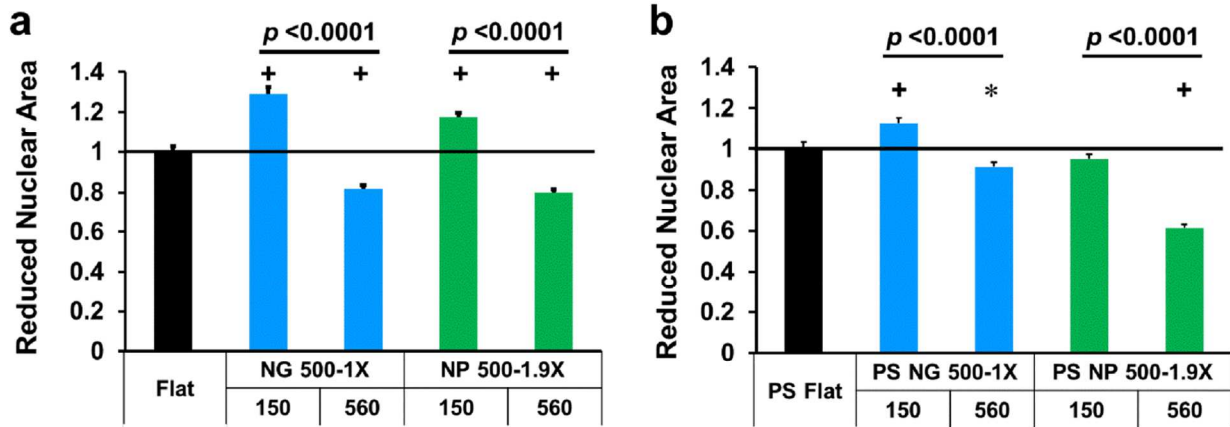


**Figure S11** Effect of nanotopography height on nuclear area of fibroblasts grown on (a) PDMS and (b) PS nanotopographies. The first and second rows of x-axis labels provide the lateral dimensions and the height (nm) of nanotopographies, respectively. Significant difference from the flat controls is indicated by \* where  $p < 0.05$  and + where  $p < 0.001$ . The  $p$  value between two groups (same lateral dimensions but different heights) is provided.

**Table S1** Comparison between the designed and measured dimensions of nanotopographies

<b>Nanotopographies</b>	<b>Designed Dimensions (nm)</b>		<b>Measured Dimensions (nm)</b>	
	Width	*Spacing	Width	Spacing
<b>Nanogratings</b>				
300-1X	300	300	315 ± 16	294 ± 7
300-3X	300	900	284 ± 17	901 ± 7
500-1X	500	500	504 ± 15	485 ± 17
500-3X	500	1500	492 ± 17	1520 ± 13
1000-1X	1000	1000	1015 ± 18	980 ± 15
1000-3X	1000	3000	1008 ± 12	2993 ± 9
<b>Nanopillars</b>	<b>Diameter</b>	<b>*Spacing</b>	<b>Diameter</b>	<b>Spacing</b>
300-1.3X	300	90	299 ± 15	130 ± 37
300-1.9X	300	270	302 ± 10	262 ± 20
500-1.3X	500	150	510 ± 8	154 ± 12
500-1.9X	500	450	487 ± 11	456 ± 10
1000-1.3X	1000	300	1012 ± 13	318 ± 25
1000-1.9X	1000	900	976 ± 19	897 ± 13

\* the edge-to-edge spacing for NGs and the center-to-center spacing for NPs